Discrete Element Simulations of Shallow Plate-Load Tests

Zhongzhi Fu[1]; Shengshui Chen[2]; and Sihong Liu[3]

Abstract: Shallow plate-load tests were simulated using a two-dimensional discrete element procedure together with parameters calibrated from a series of biaxial compression experiments on aluminum rods. The deformation and force transmission characteristics within ground materials were investigated first, and then attentions were focused on studying the influences of the interparticle friction coefficient, the roughness of the loading plate, and the size of loading plate on the testing results, including the ultimate bearing capacity, the deformation behavior, and the failure mode. The well-known scale effect in plate-load tests was also analyzed from the perspectives of both continuum mechanics and discrete element method simulations. It was proven that the nonlinear strength behavior of the materials beneath the foundation is a possible source of the scale effect; however, this effect may be counterbalanced by the boundary restriction effect in laboratory experiments. **DOI: 10.1061/(ASCE)GM.1943-5622.0000588.** *© 2016 American Society of Civil Engineers.*

Author keywords: Discrete element method (DEM); Plate-load test; Bearing capacity; Failure mode; Scale effect.

Downloaded from ascelibrary.org by Hohai University Library on 01/17/16. Copyright ASCE. For personal use only; all rights reserved.

Introduction

The plate-load test is a type of in situ experiment performed on a foundation to estimate the bearing capacity and the modulus of the underlying soil. The test results are quite useful in designing foundations for which the permitted load and the settlement of the foundation should be determined. Despite the fact that a plate-load test can give information on the soil to a depth equal to only approximately 2 diameters of the bearing plate (ASTM 2003), the method can be extremely helpful in gravelly soils in which undisturbed sampling is not possible, provided it is preceded by a borehole program, to prove that the soil does not exhibit significant variations (Smith and Smith 1998). In general, no less than three different representative locations should be selected and tested so that the possible inhomogeneity of the foundation materials can be recognized and a sensible average can be made on the obtained parameters (ASTM 2003).

Although the plate-load test method is routinely used in geotechnical engineering, the test results should be interpreted and used with caution, because these results are evidently influenced by both the plate width (known as the scale effect) (De Beer 1965; Cerato and Lutenegger 2007; Loukidis and Salgado 2011; Zhu et al. 2001; Ueno et al. 2001) and the boundary conditions (Yamaguchi et al. 1976; Cerato and Lutenegger 2006). Various tests and numerical results have shown that the scale effect may be attributed to the presence of matric suction (Oh and Vanapalli 2013; Costa et al. 2003), the nonlinearity of the Mohr-Coulomb failure envelope (Cerato and Lutenegger 2007; Hettler and Gudehus 1988; Loukidis and Salgado 2011; Zhu et al. 2001; Ueno et al. 2001), and progressive failure along the slip surfaces (Yamaguchi et al. 1976; Consoli et al. 2009; Loukidis and Salgado 2011). The particle size effect was also interpreted as one of the sources for the dependence of the bearing capacity on footing size (Herle and Tejchman 1997; Tatsuoka et al. 1991).

Recently, Cerato and Lutenegger (2007) tried to explain the scale effect by virtue of the critical state concept, and they suggested that for a model-scale test to be representative of a larger full-scale test, it must be performed on sand that is looser than the sand underneath that of the full-scale test so that the distances from the state points to the critical state line on the mean stress ~ void ratio diagram are the same for both cases. Although the critical state concept was proven to be powerful in explaining the scale effect (Cerato et al. 2007), no applicable quantitative criterion has been proposed yet to guide the preparation of model tests. To establish principles that take the scale effect into account, much effort has been devoted to modifying bearing-capacity factors (Hettler and Gudehus 1988; Shiraishi 1990; Loukidis and Salgado 2011; Zhu et al. 2001; Ueno et al. 2001; Consoli et al. 2009; Consoli et al.1998) so that the empirical formula established can also be extrapolated to full-scale footings.

The failure mechanism of the foundation system was studied conventionally by either optical observations from the vertical boreholes excavated below the plates after testing (Consoli et al. 2009) or tracking the deformation processes of the soil mass in a physical model using modern electronic devices (Yamaguchi et al. 1976; Matsuoka and Liu 2005). With the development of numerical methods and the increase of computational capacity, the failure mechanism of foundations was also investigated in recent years by using numerical simulations (Consoli et al. 2009; Bhandari and Han 2009; Sloan 2013; Loukidis and Salgado 2011; Kumar 2009), in which more complicated loading conditions and boundary conditions could be modeled appropriately. Consoli et al. (2009) found that for a cemented soil layer overlaying a weaker layer, the tensile failure first initiates at the bottom of the cemented layer and the fractures extend upward. As loading on the test plate increases, shear failure starts to progress downward from the edge of the test plate. The tensile fractures and the shear failure finally evolve into a single vertical failure surface, producing a so-called punching failure mode. Two-dimensional discrete element simulations by Bhandari and Han (2009), however, reproduced the general shear failure mode assumed by Terzaghi (1943), although the triangle wedge under the footing was much smaller. Bhandari and Han (2009) also noticed the unsymmetrical movement of particles due to fabric

[1]Senior Engineer, Geotechnical Engineering Dept., Nanjing Hydraulic Research Institute, Nanjing, Jiangsu Province 210024, China (corresponding author). E-mail: fu_zhongzhi@yahoo.com

[2]Professor, Key Laboratory of Earth-Rock Dam Failure Mechanism and Safety Control Techniques, Ministry of Water Resources, Nanjing, Jiangsu Province 210029, China. E-mail: sschen@nhri.cn

[3]Professor, Institute of Hydraulic Structures, Hohai Univ., Nanjing, Jiangsu Province 210098, China. E-mail: sihongliu@hhu.edu.cn

Note. This manuscript was submitted on November 7, 2014; approved on July 15, 2015; published online on January 5, 2016. Discussion period open until June 5, 2016; separate discussions must be submitted for individual papers. This paper is part of the ***International Journal of Geomechanics***, © ASCE, ISSN 1532-3641.

inhomogeneity. Using a two-surface plasticity constitutive model, Loukidis and Salgado (2011) reproduced the general shear collapse mechanism in their FEM, and they found that the full formation of such a collapse mechanism requires large settlement and is not strictly coincident with the attainment of peak load.

As a result of the large amounts of experimental data accumulated around the world and advances in soil constitutive models, as well as the great computational capacity available, bearing-capacity problems, including both the ultimate bearing capacity and the corresponding failure mode, can be investigated and verified with sufficient credibility by using continuum mechanics. However, investigations on the responses of the foundation system, particularly microscopic responses of the underlying soil, which may be of great importance in deepening our understanding of the macroscopic behavior, have been relatively sparse. In contrast, some of the aspects (e.g., the influence of interparticle friction on force transmission characteristics) could not be studied conveniently in continuum mechanics up to now. Considering the capability of discrete element method (DEM) simulations to shed light on the behavior of particulate systems on a particle level (Cundall and Strack 1979; Zhang and Thornton 2007; Liu et al. 2009; Fu et al. 2011), series of two-dimensional discrete element simulations of plate-load tests were conducted in this study with an aim of elucidating the following aspects:

- The deformation and force transmission characteristics within a particulate foundation system and their dependence on interparticle friction;
- The influence of plate roughness on test results, including the displacement mode of particles and the bearing capacity of the tested material; and
- The interpretation of the scale effect observed in various plate-load tests, in which the foundation material exhibits a nonlinear strength behavior.

Despite the capability of the DEM for modeling both cohesive and cohesionless soils, only cohesionless materials were considered in this study, because most of the previous experimental studies were performed with sands, which exhibit an evident nonlinear strength property. Before simulating the plate-load tests, the required DEM parameters were calibrated on the basis of biaxial compression experiments on aluminum rods, as presented in the next section. Throughout this study, for the sake of simplicity in interpretation of the results, no suction effect was considered.

Calibration of DEM Parameters

Biaxial Compression Tests on Aluminum Rods

Biaxial compression tests on aluminum rods were conducted in the laboratory at the Institute of Hydraulic Structures, Hohai University. Fig. 1 shows a plot of the biaxial compression apparatus, which was composed mainly of horizontal and vertical loading frames, top and side electric motors, load transducers, and a controlling unit. The rectangular specimen, with a width of 110 mm and a height of 220 mm, was prepared by mixing aluminum rods with two different radii (1.5 and 3.0 mm; the area ratio between both groups was 3:2). These rods were trimmed from stretched aluminum wires and had a uniform length of 50 mm. Note that aluminum rods were used because their specific gravity (≈ 2.69) is similar to that of real granular soil particles (≈ 2.65); consequently, their behavior under loading could be seen as an ideal analog of cohesionless soil behavior (Liu et al. 2009; Delenne et al. 2004). To represent the experimental specimen, a numerical specimen (110×220 mm), which is composed of 5,322 disks with a diameter of 1.5 mm and 888 disks with a diameter of 3.0 mm, was also generated using the DEM program mentioned in the subsequent section. Sufficient attention was paid to the numerical specimen so that its initial void ratio is almost the same as that of the experimental one (i.e., $e_0 \approx 0.22$).

The procedure of biaxial compression experiments was similar to that of triaxial compression tests. First, confining pressure was applied to the specimen by setting the lateral and vertical forces according to the dimensions of the specimen. Then, additional vertical load was exerted on the top surface of the specimen while keeping the lateral load constant. Fig. 2 shows the typical experimental results obtained under four different confining pressures (i.e., 50, 100, 150, and 200 kPa); the black and bright triangles and circles represent experimental data, and the curves represent relevant results obtained from DEM simulations.

DEM Parameters Calibrated from Biaxial Compression Tests

For the calibration of DEM parameters and all the simulations conducted hereafter, the DEM code DEAPERS (Discrete Element Analysis Program for Earth and Rockfill Structures), originally

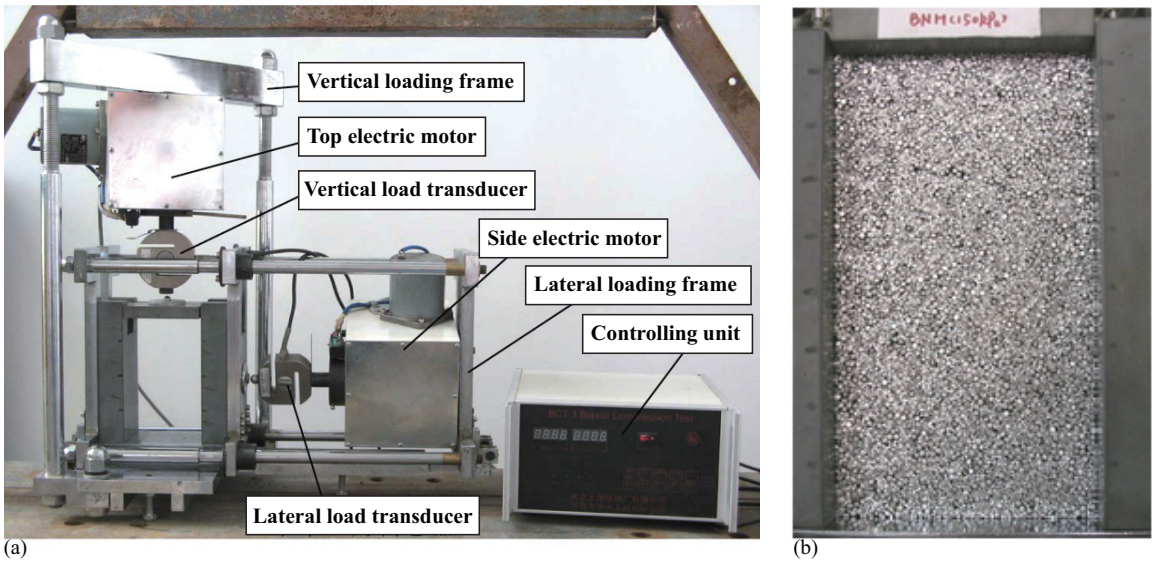

Fig. 1. (a) The biaxial compression apparatus; (b) the specimen ($e \approx 0.22$)

Downloaded from ascelibrary.org by Hohai University Library on 01/17/16. Copyright ASCE. For personal use only; all rights reserved.

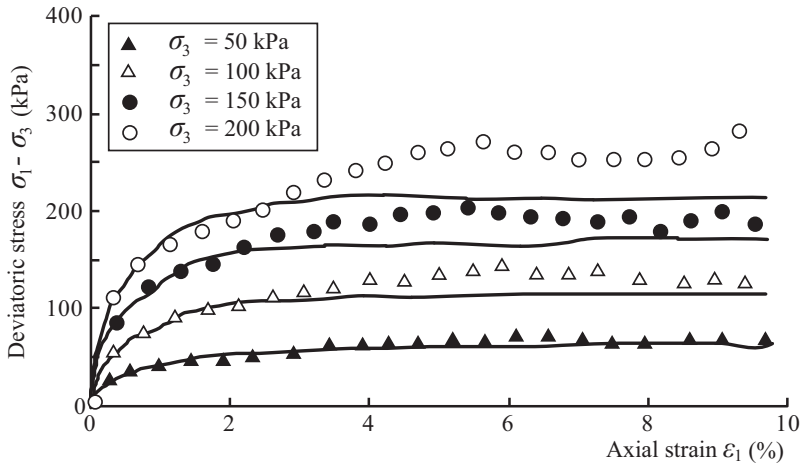

Fig. 2. Typical results obtained from biaxial compression tests on aluminum rods (triangles and circles indicate experimental data, and curves represent DEM simulation results)

developed and continuously updated by the authors, was used. This program has been used successfully for studying wetting effects on granular materials (Fu et al. 2011). More recently, it was also used for studying the microscopic interpretation of the yield surface in elastoplasticity (Liu et al. 2015).

Similar to other DEM codes, conducting simulations using DEAPERS requires three groups of parameters (i.e., particle parameters, contact parameters, and kinematic parameters). The particle parameters include the densities of different particles, and they were uniformly scaled up to 2.7×10^4 kg/m^3 throughout this study. The contact parameters include the friction coefficient between contacting particles and the normal and tangential stiffness. The kinematic parameters herein refer to the viscous damping coefficients, which specify the resistant force and moment proportional to the translational and rotational velocities of particles. Contact damping was also widely used in the DEM to calculate the contact forces proportional to the relative velocities of contacting particles (Liu et al. 2009; Liu and Sun 2002). In fact, both types of damping can be used in a combined way. However, the latter was not used in this study, because including such an effect will introduce more parameters and inevitably complicate the calibration. In contrast, the only influence of contact damping was the magnitude of contact forces between contacting particles, which can be reflected via the calibration of normal and tangential stiffness (i.e., neglecting contact damping will not sacrifice the credibility of DEM simulations) (Fu et al. 2011).

In many back-analysis problems, the parameters can be determined by using an optimization algorithm in which the optimal solution is searched automatically. However, in DEM simulations, optimization can currently be done only by manually adjusting the most influencing parameters and following a trial-and-error method because of the high computational cost in time. Table 1 lists the parameters calibrated in this way from the biaxial compression tests, and results of the comparison of numerical and experimental results are shown in Fig. 2. Satisfactory agreement was observed for most of the obtained results, except for the one conducted under the confining pressure of 200 kPa, which seems to prove the rationality of the results listed in Table 1. It should be pointed out that in all the DEM simulations, the density of particles was scaled up 10-fold and the gravity acceleration was scaled down 10-fold. As a result, the weight of particles did not change, but the time step for simulation was increased to reduce the total time cost considerably.

Table 1. DEM Parameters Calibrated from Biaxial Compression Tests

Parameter	Calibrated value
Density of particles, ρ (kg/m^3)	2.7×10^4
Friction coefficient, μ	0.2
Normal stiffness, k_n (N/m)	3.0×10^8
Tangential stiffness, k_t (N/m)	1.0×10^8
Translational damping coefficient, α [N/(kg·m/s)]	100.0
Rotational damping coefficient, β [N·m/(kg·m^2·rad/s)]	10.0

Note: The balance equations of an arbitrary particle read: $F - \alpha m\dot{u} - m\ddot{u} = 0$ and $M - \beta I\dot{\theta} - I\ddot{\theta} = 0$, in which F and M = unbalanced forces and moment, respectively; m and I = mass and moment of inertia of the particle, respectively; u = displacement vector; θ = angular displacement; and α and β are two viscous damping coefficients.

Discrete Element Model for Plate-Load Tests

Preparation of the Plate-Load Test Model

The plate-load test model was prepared by filling particles with radii of 1.5 and 3.0 mm (area ratio = 3:2) from a certain height into the containing box formed by three rigid walls. The rough surface was then leveled by using a top horizontal rigid wall driven by a small downward force. After a stable state was achieved, the top wall was removed, and the rigid loading plate, formed by four short rigid walls, was placed on the surface of the particles along the center of the containing box. Fig. 3 shows the setup of the DEM model, in which several rows and columns of particles were colored to facilitate the trace of their movement and the exploration of the deformation mode under the loading plate.

To evaluate the homogeneity and isotropy of the initial state, the vertical and horizontal void ratios of the DEM model were evaluated according to the following equations:

$$e_V = \frac{H - \sum l_i}{\sum l_i}; \quad e_H = \frac{W - \sum l_i}{\sum l_i} \tag{1}$$

in which H and W represents the height (250 mm) and the width (1,000 mm) of the DEM model, respectively. l_i denotes the length at which the ith particle intersects the scanning line as shown in

Downloaded from ascelibrary.org by Hohai University Library on 01/17/16. Copyright ASCE. For personal use only; all rights reserved.

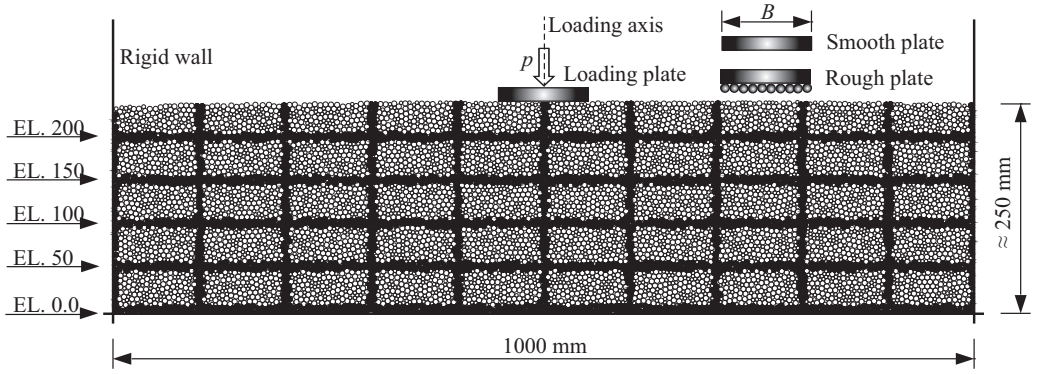

Fig. 3. Setup of DEM plate-load tests

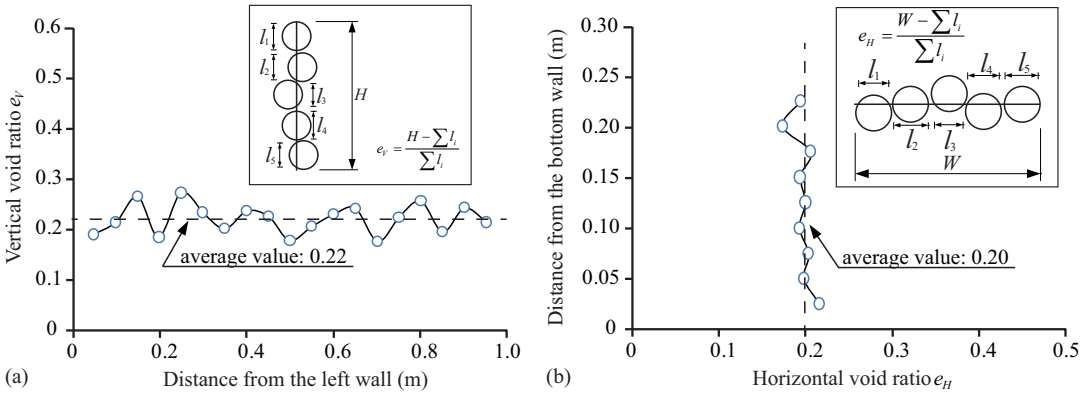

Fig. 4. Directional void ratios within ground in the DEM model: (a) vertical void ratio; (b) horizontal void ratio

Table 2. Investigated Cases and Their Purpose and Condition

Group number	Purpose	Particular condition
PLT1	Basic case for force transmission and deformation mode	Parameters in Table 1 ($\mu = 0.2$); plate width = 100 mm
PLT2	Influence of interparticle friction	$\mu = 0.4$ and 0.6
PLT3	Influence of plate roughness	Rough loading plate; $\mu = 0.2$ and 0.4
PLT4	Influence of plate width (the so-called scale effect)	Plate width = 50 and 200 mm; $\mu = 0.2$ and 0.4

Note: In PLT1, PLT2, and PLT4, a smooth plate was used, and the friction between the plate and the underlying particles was neglected.

Fig. 4. Given the direction and location of the scanning line, the vertical void ratio, e_V, and the horizontal void ratio, e_H, are in essence the ratio between the unintersected portion and the intersected portion. Fig. 4 shows the distributions of the vertical and the horizontal void ratios evaluated by using Eq. (1). The vertical void ratio exhibits a certain fluctuation around an average value of 0.22, whereas the horizontal void ratio fluctuates less evidently around an average value of 0.20. These results indicate that the DEM model is not ideally homogeneous, especially along the horizontal direction. Furthermore, the fact that the average e_V is higher than the average e_H in Fig. 4 implies that a certain fabric anisotropy also exists in the model despite the regular particle shape. These inhomogeneity and anisotropy effects were also noticed by other authors (Bhandari and Han 2009; Sanchez et al. 2015) and are rather difficult to control. In contrast, neither homogeneity nor isotropy is guaranteed strictly in physical modelling. Therefore, we continued to use this DEM model for the following investigations.

Four series of simulations were carried out in this study, and the purposes of each group and the corresponding condition are summarized in Table 2. PLT1 was the basic case in which the parameters listed in Table 1 were used to study the force transmission characteristics and the deformation mode in a load test, which has a plate width of 100 mm. PLT2 altered the interparticle friction coefficient μ to investigate the influence of interparticle friction on the test results. The influence of the plate roughness was studied in PLT3, in which a rough plate was represented by attaching a layer of particles to the bottom of the loading plate, as was done in laboratory experiments (Cerato and Lutenegger 2007; Yamaguchi et al. 1976). PLT4 was focused on the scale effect, widely recognized in plate-load tests; the loading plate widths were changed to 50 and 200 mm. In all these simulations, two smooth vertical side walls were attached to the loading plate to prevent the heaving particles from moving toward the loading axis.

Computational Issues in Numerical Simulations

The loading was modeled by specifying a downward velocity to the loading plate, because the ultimate bearing capacity of the foundation could not be estimated a priori (i.e., the force-driven mode was not suitable, and therefore the displacement-driven mode was

Downloaded from ascelibrary.org by Hohai University Library on 01/17/16. Copyright ASCE. For personal use only; all rights reserved.

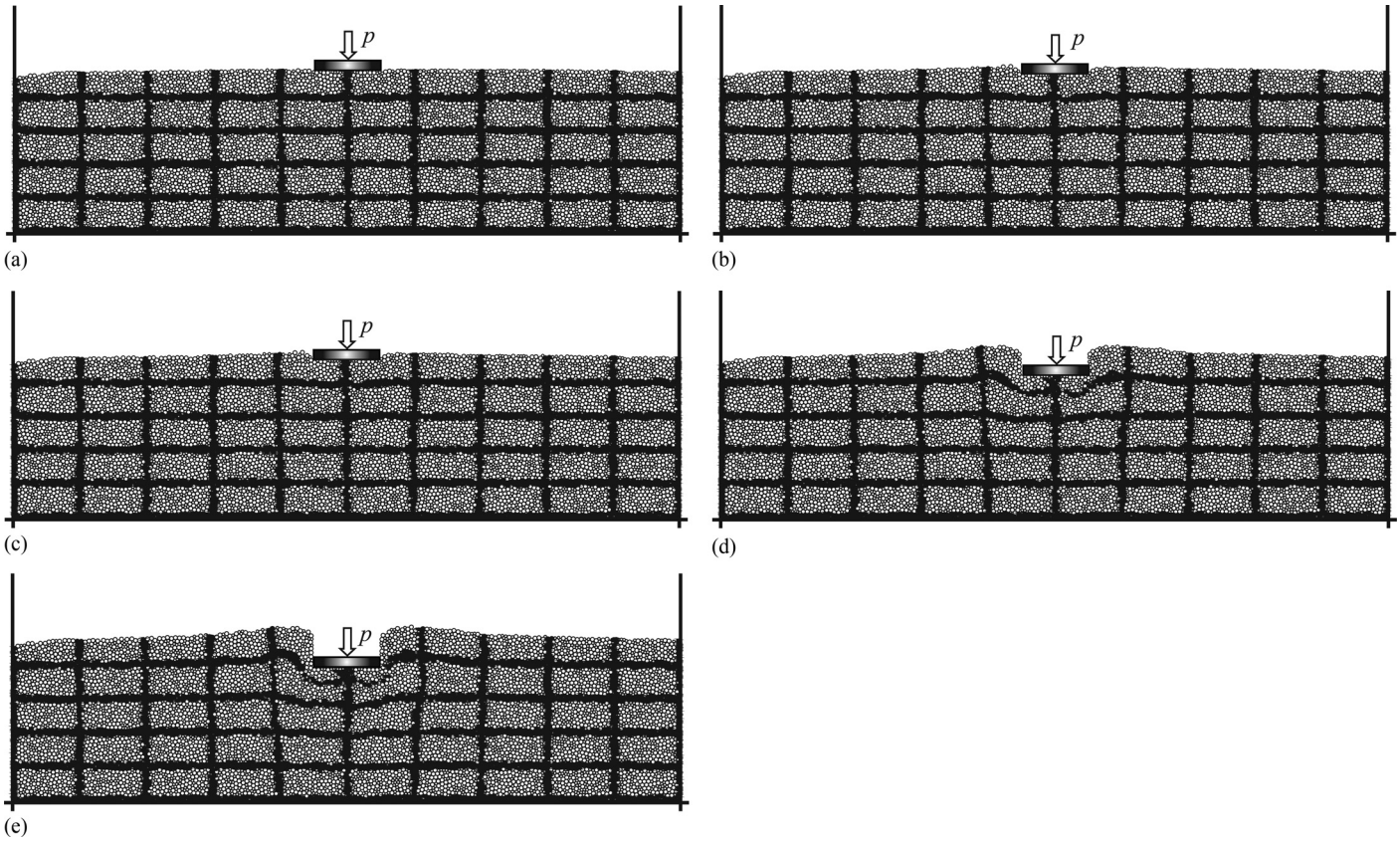

Fig. 5. Deformation processes of the foundation in PLT1: (a) $p = 40$ kPa; (b) $p = 80$ kPa; (c) $p = 120$ kPa; (d) $p = 160$ kPa; (e) $p = 200$ kPa

adopted). In DEM simulations, contact identification is the most time-consuming process, and several techniques have been proposed to reduce the time cost, such as the cell-searching technique and the density-scaling technique (Itasca Consulting Group 1999). Herein, both the cell-searching technique and the density-scaling technique were used, and the contact identification within each cell was parallelized using *OpenMP* (Hermanns 2002; Fu et al. 2014).

Another important issue in DEM simulation is the choice of time increment Δt, and the results of a single degree of freedom (SDOF) dynamic system could be referred (Chopra 2009). The natural period of a free vibrating SDOF system reads as follows:

$$T = 2\pi\sqrt{\frac{m}{k_n}} \tag{2}$$

For the smallest particle (1.5 mm), the period was estimated to be approximately 1.6×10^{-4} s. Hence, the time increment Δt was set in this study to 1×10^{-5} s ($T/16$), and the total duration of the loading processes was 5.0 s in all of the previously mentioned cases.

Results and Discussion

Deformation and Force Transmission Characteristics

Fig. 5 plots the deformation processes of the soil beneath the loading plate in PLT1. The soil layer underneath the plate was compacted as soon as the external loading increased. Meanwhile, horizontal expansion, indicated by the colored particle columns, can be seen within the columns near the loading axis, which, in turn, results in heaving and loosening of the granular particles near the edges of the loading plate. These numerical results are in good agreement with experimental and in situ observations (Yamaguchi et al. 1976; Matsuoka and Liu 2005; Cerato and Lutenegger 2006). In addition, the horizontal expansion of higher layers (underneath the plate) is much more evident than that in lower layers, indicating that vertical compaction decreased with increasing depth from the plate base, and there existed a threshold depth below which the particles were almost not disturbed by the loading. It can be inferred from Fig. 5 that the threshold depth herein was approximately twice the width of the plate, because the configuration of the bottom layer, throughout the loading process, was almost the same as that in the initial state.

Fig. 6 shows a plot of the distribution of average normal contact force at different elevations (EL) (i.e., 0.0, 50, 100, and 150 mm). The average normal contact force at each layer was calculated by averaging the contact forces at all those contacting points within a selecting box (length × height = 50 × 20 mm), the center of which moves from the left wall at the concerned elevation to the right wall with a horizontal interval of 50 mm, that is

$$\bar{F}_n = \frac{1}{N_c}\sum_{i=1}^{N_c} F_{ni} \tag{3}$$

in which F_{ni} = normal contact force at ith contacting point; and N_c = total number of contacting points within the selecting box. The average forces at all the elevations followed almost but not strictly symmetrical distribution, indicating that the numerical sample contained by the rigid walls was almost but not ideally homogeneous, as mentioned previously. It can also be seen in Figs. 6(c and d) that the normal contact force was concentrated beneath the loading plate. However, the intensity of force concentration decreased when the depth of the layer to the plate base increased.

Downloaded from ascelibrary.org by Hohai University Library on 01/17/16. Copyright ASCE. For personal use only; all rights reserved.

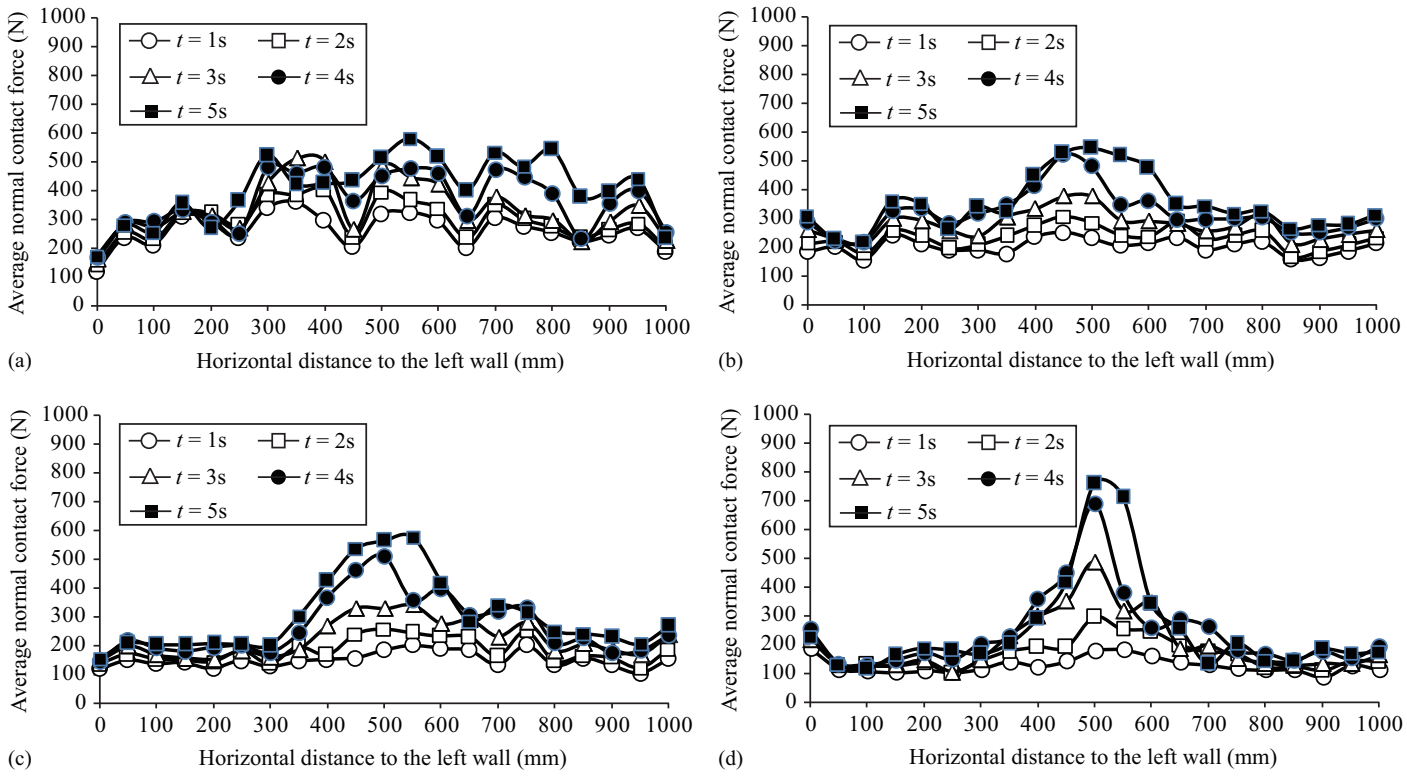

Fig. 6. Distributions of the average normal contact force at different elevations: (a) EL 0.0 mm; (b) EL 50.0 mm; (c) EL 100.0 mm; (d) EL 150.0 mm

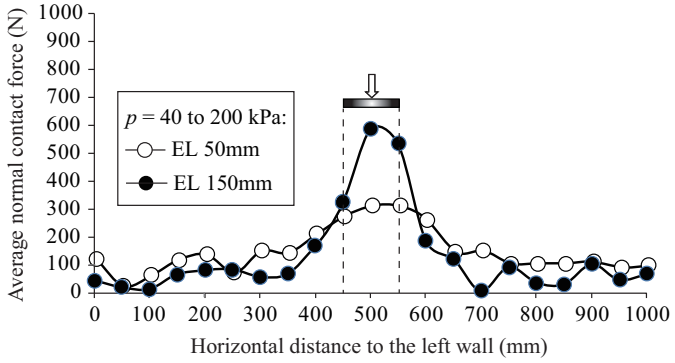

Fig. 7. Increase of the average normal contact force

Fig. 7 shows the increase of average normal contact forces at $p = 40$–200 kPa at EL 50 and 150 mm. By plotting the incremental normal forces, the influence of initial state was eliminated. Although the average normal contact force increased much more at EL 150 mm within zones right under the loading plate compared with that at EL 50 mm, the latter had a higher increase in the average contact force within zones outside the loading plate. Namely, the force distribution diagram is much flatter at lower levels. This force transmission feature indicates that the area influenced by the vertical loading increased with the depth, although the magnitude of the induced disturbance decreased with increasing depth (see Fig. 7).

Influence of Interparticle Friction on the Test Results

Fig. 8(a) plots the settlement against the vertical pressure obtained by DEM simulations with three different interparticle friction coefficients (i.e., $\mu = 0.2,\ 0.4,$ and 0.6). Each curve presents an initial curved portion and continues to descend on a slope of slightly different inclination. Terzaghi (1943) postulated that the foundation fails as soon as the curve passes into a steep and fairly straight tangent. However, in many practical problems, the intersection of the curved portion and straight slope is not very clear. What is worse is that the pressure-versus-settlement curve sometimes differs totally from the one suggested by Terzaghi (1943), as exemplified by Fig. 8(b), which were results of plate-load tests carried out on the overburden layer of a rockfill dam (Fu and Huo 2013). Therefore, a settlement criterion is often adopted instead to define the bearing capacity. In this study, the pressure in accordance with a settlement ratio S/B (B denotes the width of loading plates) of 0.1 was interpreted as the bearing capacity, as suggested in the literature (Cerato and Lutenegger 2007; Cerato and Lutenegger 2006; Hisham 2013). Fig. 8(a), shows clearly that a higher interparticle friction results in an enhanced deformation modulus and also a higher bearing capacity.

Fig. 9(a) shows the probability density distribution of normal contact forces between particles at the instant that the plate pressure is 100 kPa. The probability was evaluated by dividing the number of contacts that carry normal forces within a given range by the total number of contacts. The accumulated probability distribution is shown in Fig. 9(b). Similar to the grain size distribution in soil mechanics, the accumulated probability is defined as the percentage of contacts that carry normal forces higher than the value specified by the abscissa. It can be seen that the variation in interparticle friction coefficients does not result in an evident change of the (accumulated) probability density distribution. In all three cases, the probability (percentage of contacts) decreased with the increase of the specified normal contact force. Approximately 90 percent of the contacts carried normal forces less than 500 N, and only the remaining 10 percent of contacts carried a load higher

Downloaded from ascelibrary.org by Hohai University Library on 01/17/16. Copyright ASCE. For personal use only; all rights reserved.

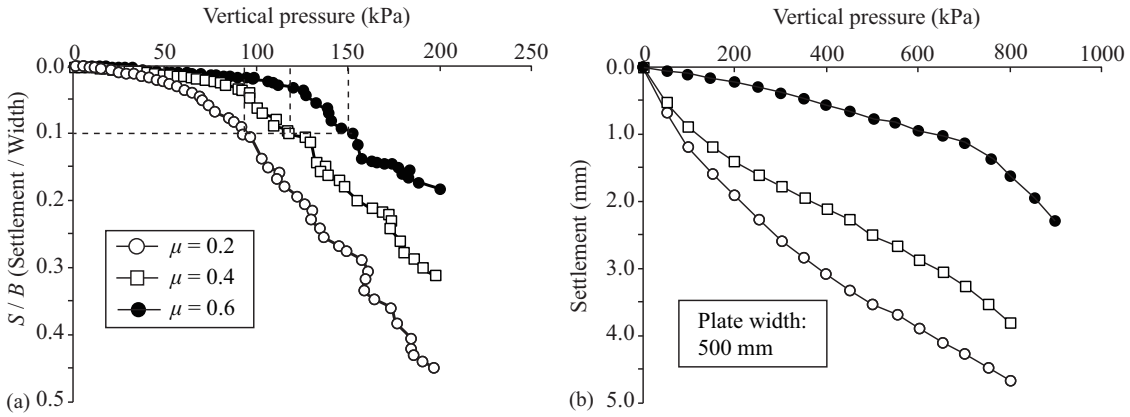

Fig. 8. Vertical pressure versus settlement: (a) DEM simulations; (b) in situ tests (from Fu and Huo 2013)

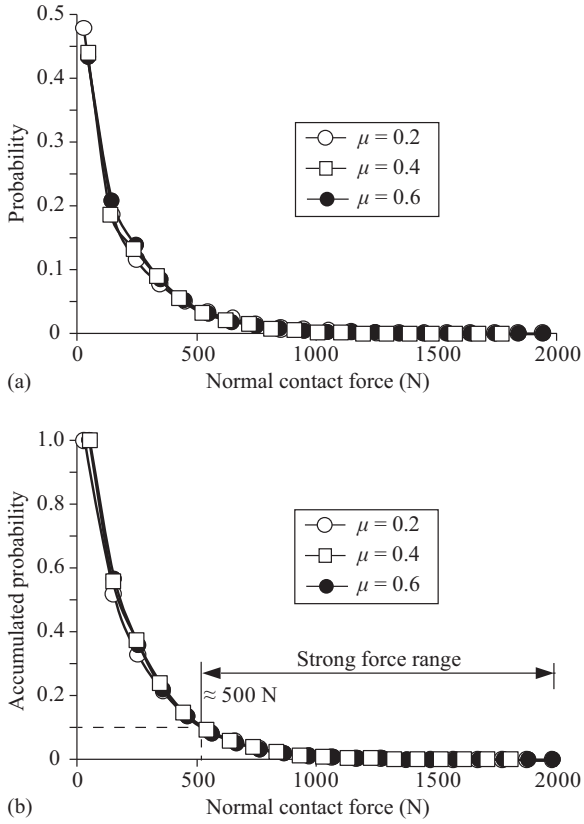

Fig. 9. Distributions of normal contact force: (a) probability density distribution; (b) accumulated probability distribution

than this value. Sun and Wang (2009) also found that within a loaded granular medium, only a few contacts carry extremely high normal forces, and they connected these contacting particles to represent the so-called strong force chains. In this study, a strong force range, in which only 10% of contacts bear normal forces within this range, was defined to select strong force contacts, as shown in Fig. 9(b).

Fig. 10 depicts the strong force chains that were formed by connecting the contacting particles on which the normal contact forces exceeded 500 N at the instant that the plate pressure was 100 kPa. The strong force chains in all three cases distributed primarily within trapezoidal zones, the slope of which increases when the interparticle friction coefficient is increased, that is, higher interparticle friction leads to a lower expansion angle of particle forces and thus a smaller strongly disturbed zone. This conclusion is easy to understand; imagining that the material contained by rigid walls is water and now applying a vertical force to a wooden rectangular plate until it is submerged, the pressure exerted on all the water particles below the lower surface of the wooden plate increases simultaneously with the same magnitude. In contrast, if the bearing area is built with bricks without interlocking, compressing one column of them will generally not influence others.

Influence of Plate Roughness on Test Results

Not only the interparticle friction coefficients but also the friction between the loading plate and underlying granular particles has an appreciable influence on the test results (Meyerhof 1955; Kumar 2003; Kumar 2004; Kumar 2009). Fig. 11 compares the numerical results obtained from DEM plate-load tests performed with smooth and rough plates. It can be seen that both the deformation modulus and the bearing capacity are higher when the loading plate is rough than those with a smooth plate. This conclusion is in accordance with the results derived from the perspective of continuum mechanics (Meyerhof 1955; Kumar 2009).

Fig. 12(a) shows the displacement vector of particles driven by a smooth plate (PLT1). The particles underneath the plate displaced downward and almost symmetrically toward both sides of the model container. This displacement mode is the so-called Hill mechanism (Chen and Liu 1990) (i.e., the failure surface initiates from the center of the plate, and no trapped wedge can be observed clearly). Meyerhof (1955) also suggested such a symmetrical failure mechanism without inclusion of any nonplastic wedge below the base for a smooth footing. Recently, a similar failure mechanism was validated by using the method of characteristics (Kumar 2009; Veiskarami et al. 2014). Fig. 12(b) plots the displacement vector obtained for a rough plate-load test. Friction between the particles and the plate base seemed to restrict the particles under the plate from moving toward the left and right sides of the container in a symmetrical manner. Instead, there was a right-triangle-shaped region within which the particles moved toward the bottom-right corner of the container; however, no counterpart triangular zone was observed within which the particles moved symmetrically toward the bottom-left corner. This result may be attributed to the initial fabric anisotropy of the particulate system (Bhandari and Han 2009; Sanchez

Downloaded from ascelibrary.org by Hohai University Library on 01/17/16. Copyright ASCE. For personal use only; all rights reserved.

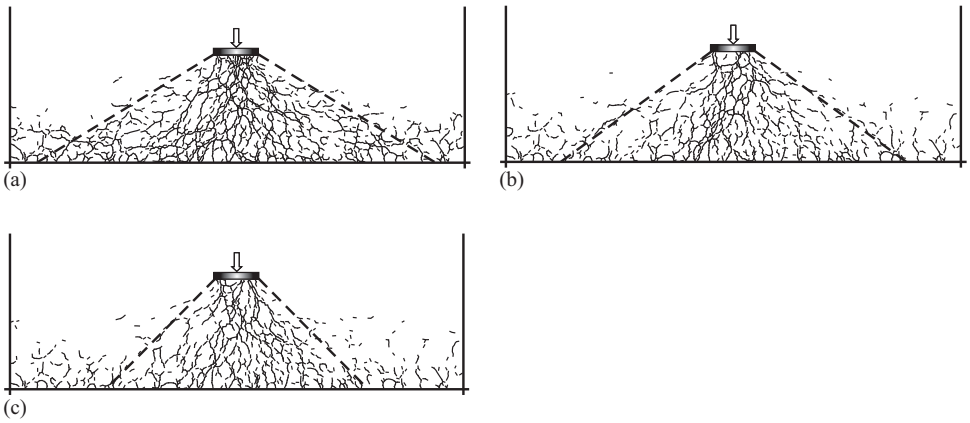

Fig. 10. Strong force chains ($F_n > 500$ N) under different friction coefficients ($p = 100$ kPa): (a) $\mu = 0.2$; (b) $\mu = 0.4$; (b) $\mu = 0.6$

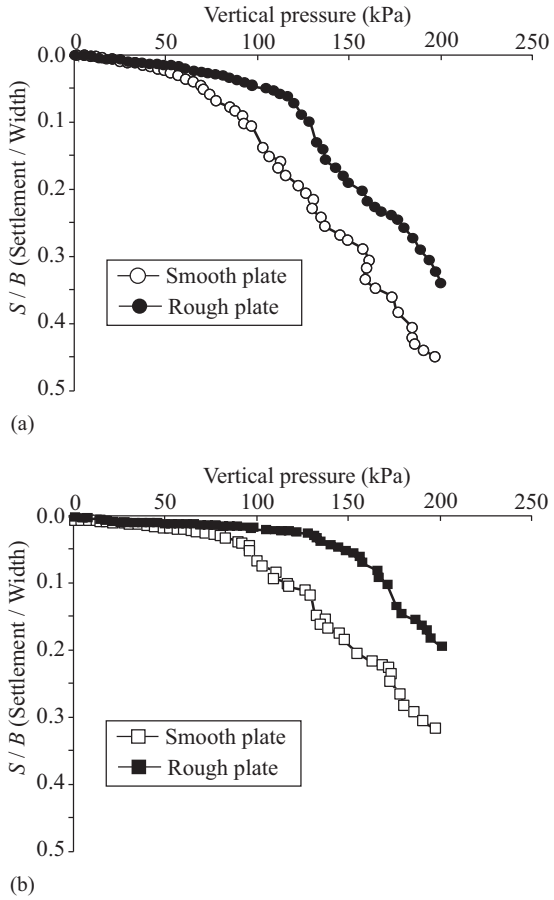

Fig. 11. Comparison of numerical results based on smooth and rough plates: (a) $\mu = 0.2$; (b) $\mu = 0.4$

et al. 2015) and hints that the failure surface is a combination of a linear segment and a curved segment, as shown in Fig. 12(b). These microscopic DEM observations are also in good agreement with the analytical results based on continuum mechanics (Meyerhof 1955; Kumar 2009; Chen and Liu 1990; Veiskarami et al. 2014). DEM simulations for particulate systems seem to be of potential value in establishing the compatible failure mode and velocity field for limit-equilibrium analysis and upper-limit analysis of strength problems (Chen and Liu 1990; Sloan 2013).

Interpretation of the Scale Effect

The scale effect in bearing-capacity problems generally refers to the nonproportional increase of the ultimate bearing capacity with the increase of footing width or decreasing bearing-capacity factor, N_γ, with the increase of footing width (De Beer 1965; Cerato and Lutenegger 2007; Zhu et al. 2001; Ueno et al. 2001). One important point that must be clarified is the definition of the ultimate state of the system. In general, in geotechnical problems, the ultimate state is controlled by either the strength of the materials used or the allowed deformation of the system. If the bearing capacity is controlled by the allowed deformation, then the nonlinear dependence of bearing capacity on the plate width lies essentially in the nonlinear deformation behavior of the underlying material. In contrast, if the shear strength of ground material governs its bearing capacity, then the scale effect boils down to the nonlinear strength behavior of the underlying material. Herein, we considered the latter case (nonlinear strength problem) from the perspective of continuum mechanics and the former case (deformation-limiting problem) by using DEM simulations.

Fig. 13 shows an illustrative example in which the bearing capacity for four different sizes of footing (i.e., 0.5, 1.0, 1.5, and 2.0 m) were estimated by using the limit-equilibrium method proposed by Chen and Morgenstern (1983) for stability problems. The ultimate bearing capacity was determined by an iterative procedure to ensure that the stability factor, F_s, of the system was 1.0. For the sake of simplicity, circular slip surface was assumed to represent the failure mechanism, as was also done by Sloan (2013) in limit analysis. The Mohr-Coulomb strength used herein was $c = 0$; $\varphi = 24^\circ$ (Jiang 2009) and no dependence of the friction angle on the confining pressure were considered. Note that the simple Mohr-Coulomb failure criterion, which neglects the influence of the intermediate principal stress, was adopted because two-dimensional problems were considered in this study. As can be seen in Fig. 13, all the slip surfaces intersect the horizontal ground surface at an angle of approximately 57° ($45^\circ + \varphi/2$), which seems to validate the reliability of the obtained results. It can also be seen in Fig. 13 that both the bearing capacity and the depth of sliding mass increase proportionally with the increase of footing width, which agrees exactly with the classical soil mechanical solutions (Terzaghi 1943; Chen and Liu 1990). That is to say, if the bearing capacity of the foundation is controlled by the strength of the underlying material and no dependence of its friction angle on the normal stress exists, then no scale effect will present regarding the bearing capacity and the footing width.

Downloaded from ascelibrary.org by Hohai University Library on 01/17/16. Copyright ASCE. For personal use only; all rights reserved.

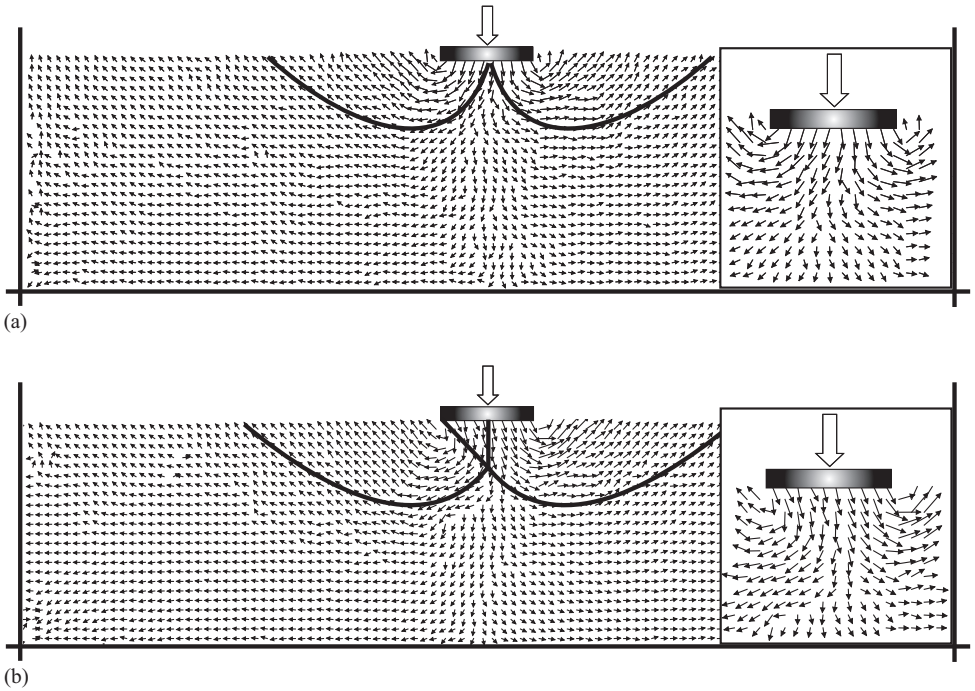

Fig. 12. Displacement vector of particles under the plates ($\mu = 0.2$ and $S = 0.1B$): (a) smooth plate; (b) rough plate

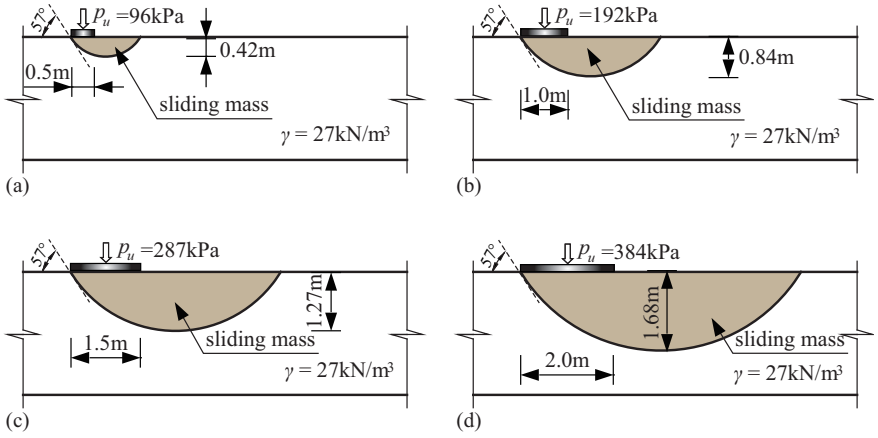

Fig. 13. Ultimate bearing capacity and corresponding sliding mass with constant strength parameters ($c = 0$ and $\varphi = 24^\circ$): (a) $B = 50$ mm; (b) $B = 100$ mm; (c) $B = 150$ mm; (d) $B = 200$ mm

However, if the internal friction angle of the underlying soil material shows an evident dependence on the normal stress, scale effect will inevitably present. To demonstrate this statement, we assume that the friction angle, φ, depends on the normal stress, σ, nonlinearly as follows (Zhu et al. 2001):

$$\varphi = \varphi_0 - \Delta\varphi \log 10\left(\frac{\sigma}{p_a}\right) \tag{4}$$

in which φ_0 and $\Delta\varphi$ = two parameters ($\varphi_0 = 24^\circ$ and $\Delta\varphi = 4^\circ$); and p_a = atmospheric pressure (101.325 kPa). The bearing-capacity problem was resolved, and the obtained results are shown in Table 3.

The introduction of two nonlinear strength parameters altered the location of slip surfaces and resulted in a considerable change of the ultimate bearing capacity and the depth of failure surface. In addition, the angle between the slip surface and the ground surface was also changed, and no unique value exists for all footing sizes. The smaller the footing is, the higher the intersection angle is. Fig. 14(a) shows the relationship between bearing capacity and footing size by using the numerical results shown in Table 3. The nonproportional increase of the bearing capacity with the increase of footing size can be seen more clearly for the nonlinear strength case. This simple example illustrates that the nonlinearity of the Mohr-Coulomb failure envelope really takes a responsibility for the observed scale effect in in situ plate-load tests.

Fig. 15 shows the DEM simulation results from experiments performed with three different sizes of loading plates (i.e., $B = 50$, 100, and 200 mm). Because in most cases the pressure-versus-settlement ($p - s$) curves do not show an abrupt change of the slopes, and thus

Downloaded from ascelibrary.org by Hohai University Library on 01/17/16. Copyright ASCE. For personal use only; all rights reserved.

Table 3. Bearing Capacity and Depth of Failure Surface for Different Plate Sizes

Friction parameters	$B = 50$ mm		$B = 100$ mm		$B = 150$ mm		$B = 200$ mm	
	p_u (kPa)	Depth (m)	p_u (kPa)	Depth (m)	p_u (kPa)	Depth (m)	p_u (kPa)	Depth (m)
$\varphi_0 = 24°, \Delta\varphi = 0°$	96	0.42	192	0.84	287	1.27	384	1.68
$\varphi_0 = 24°, \Delta\varphi = 4°$	117	0.45	198	0.93	276	1.23	340	1.58

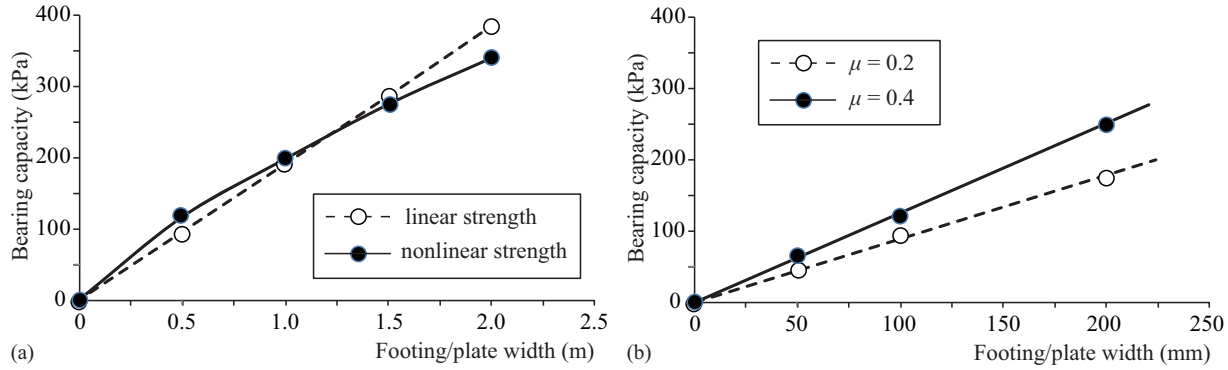

Fig. 14. Ultimate bearing capacity versus footing width: (a) limit-equilibrium analysis; (b) DEM simulations

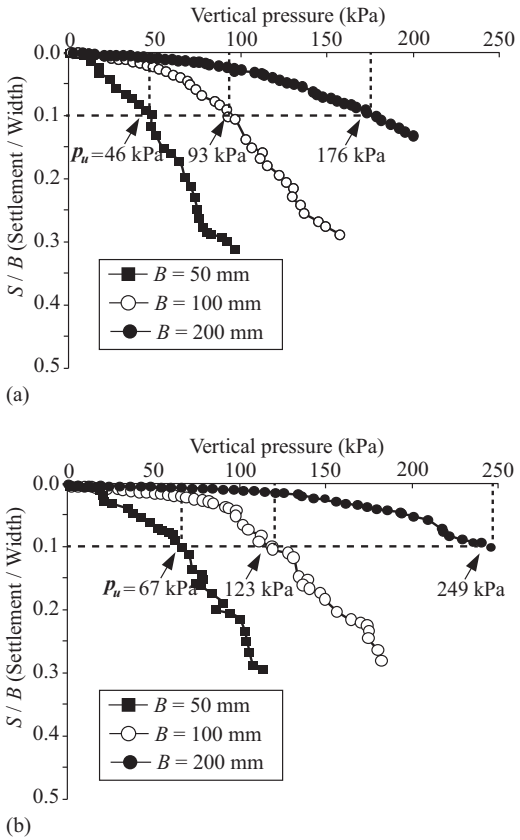

Fig. 15. Comparison of numerical results obtained with different loading plate sizes: (a) $\mu = 0.2$; (b) $\mu = 0.4$

the failure state cannot be clearly defined as by Terzaghi (1943), the pressure corresponding to a settlement ratio of 0.1 ($S/B = 0.1$) was taken to be the bearing capacity, as already mentioned. It can be seen that the $p - s$ curves of the larger plate are smoother than those of the smaller ones, which indicates that the microscopic fabric is more stable during loading on the larger plate and also hints that the fluctuation of the $p - s$ curves in real plate-load tests may be attributable to the existence of large grains within the tested area. The bearing capacities were estimated and are plotted in Fig. 14(b) against the plate widths. Note that although the plate in the DEM simulations is much smaller than that in the limit-equilibrium analysis, the bearing capacities are shown with the same magnitudes in Figs. 14(a and b) because of the application of the density-scaling technique in the DEM simulations.

Compared with the results of the nonlinear strength case, shown in Fig. 14(a), the DEM results [Fig. 14(b)] show almost linear dependence of the bearing capacity on plate width. Two reasons may account for this finding. First, the strength nonlinearity of the assembly of aluminum rods is not as evident as that used in Fig. 14(a), the strength parameters calibrated from Fig. 2 are $\varphi_0 = 24°$ and $\Delta\varphi = 2°$, and the value of the second parameter is only half of the one used in the limit-equilibrium analysis. Second, for tests with larger loading plates, the boundary effect may play a more important role in loading responses, as indicated by the denser strong force chains around the bottom and side boundaries shown in Fig. 16(b). It was demonstrated by Yamaguchi et al. (1976) that rigid boundaries (steel) resulted in higher bearing capacities and deformation moduli than those with more flexible ones (composite glass). Similarly, the boundary effect with a larger loading plate also leads to a higher bearing capacity and deformation modulus, which counterbalances the nonlinear strength effect and mendaciously yields a linear relationship between the bearing capacity and the plate width. Therefore, it is rational to infer that if the boundary effect is eliminated by using a larger container, a nonproportional increase in the bearing capacity with an increase of plate width will also be observed.

Summary and Conclusion

The results of plate-load tests are influenced by many factors, including the frictional resistance between contacting particles and the size and roughness of the loading plate. However, studying the effects of these factors is not so easy, in either field tests or

Downloaded from ascelibrary.org by Hohai University Library on 01/17/16. Copyright ASCE. For personal use only; all rights reserved.

Fig. 16. Strong force chains ($F_n > 500$ N) under different loading plates ($p = 100$ kPA): (a) $B = 100$ mm; (b) $B = 200$ mm

laboratory experiments, because of the difficulty in constructing exactly identical models. This is the well-known repeatability issue in model tests in almost all areas of experiments. In this regard, numerical experiments using discrete element simulation serve as a competitive alternative to the conventional physical model tests, particularly for those problems aimed at clarifying the most influential factors in a qualitative manner. DEM simulations also enable us to gain, to some extent, an insight into the microscopic behavior of particulate systems, which could not be obtained simply from physical model tests. In this study, series of discrete element simulations were performed, on the basis of parameters obtained from biaxial compression tests on aluminum rods, to study the influences of well-known factors on plate-load test results. The obtained results were found to be consistent with experimental and theoretical findings conducted under the framework of continuum mechanics, and the following conclusions were made:

1. In plate-load tests, the external loads are transferred to the soil layer by the force chains. The average (normal) contacting force decreases when the distance of the position to the plate base increases. Evident force concentration can be observed right under the loading plate; however, the intensity of such force concentration decreases with increasing depth, which indicates a less strongly disturbed zone at lower elevations. Graphical interpretation of the contact information indicates that the strong force chains are limited within a symmetrical trapezoidal zone.
2. The friction angle between contacting particles has a considerable influence on both the macroscopic testing results and the microscopic force transmission characteristics. An increase of the interparticle friction coefficient results in a higher bearing capacity and a higher deformation modulus. It also leads to a smaller strong contacting force zone (i.e., the slope of the symmetrical trapezoidal strong force zone becomes steeper as the interparticle friction is increased). That is to say, loading a foundation material with a higher internal friction angle induces a smaller disturbed zone than that with a lower friction angle, when measured horizontally.
3. The roughness of the loading plate has a significant influence on test results, not only on the bearing capacity but also on the failure mode of the underlying material. A smooth plate cannot restrict the particles near the base from expanding toward both sides, which finally leads to a Hill failure mechanism (i.e., symmetrical failure initiates from the center of the plate without any trapped triangular wedge). On the contrary, under the rough-plate situation, unsymmetrical failure mechanism was observed, and the failure surface was a combination of a linear segment initiated from one edge of the loading plate and a curved segment that intersected the ground surface on the other side, which reminds us that sufficient caution should be exercised when the material of the loading plate used in practice is not the same as that of the footing.
4. If the bearing capacity of the foundation is controlled by the strength of the underlying material and no nonlinear strength feature presents, then the ultimate bearing capacity and the depth of failure surface will increase proportionally with the loading plate; thus, no scale effect will present. However, most cohesionless soils (including the aluminum rods described here) have a curved Mohr-Coulomb failure envelope, and this nonlinearity in strength has been proven to be a potential source of the observed scale effect in field plate-load tests.
5. DEM plate-load tests with different sizes of loading plates show that the boundary effect may counterbalance the scale effect caused by the nonlinear strength property of soils and, thus, leads to a nearly proportional increase in the bearing capacity with an increasing plate width. Therefore, in laboratory plate-load tests with finite boundaries, special care should be taken to consider the boundary effect when interpreting the experimental results.

Acknowledgments

This work was supported by National Natural Science Foundation of China (NSFC, Grant Numbers 91215301, 51209141, and 51379130). The financial support from Nanjing Hydraulic Research Institute (NHRI, Grant Number Y314011) is also greatly appreciated.

References

ASTM. (2003). "Standard test method for bearing capacity of soil for static load and spread footings." *D 1194-94*, Philadelphia.

Bhandari, A., and Han, J. (2009). "DEM study of a shallow foundation under vertical loading." *2009 International Foundation Congress and Equipment Exposition, Contemporary Topics in Ground Modification, Problem Soils and Geo-Support*, ASCE, Reston, VA, 465–472.

Cerato, A. B., and Lutenegger, A. J. (2006). "Bearing capacity of square and circular footings on a finite layer of granular soil underlain by a rigid base." *J. Geotech. Geoenviron. Eng.*, 10.1061/(ASCE)1090-0241(2006)132:11(1496), 1496–1501.

Cerato, A. B., and Lutenegger, A. J. (2007). "Scale effects of shallow foundation bearing capacity on granular material." *J. Geotech. Geoenviron. Eng.*, 10.1061/(ASCE)1090-0241(2007)133:10(1192), 1192–1202.

Chen, W. F., and Liu, X. L. (1990). *Limit analysis in soil mechanics.* Elsevier, Amsterdam, Netherlands.

Chen, Z. Y., and Morgenstern, N. R. (1983). "Extensions to generalized method of slices for stability analysis." *Can. Geotech J.*, 20(1), 104–109.

Chopra, A. K. (2009). *Dynamics of structures theory and application to earthquake engineering*, 3rd Ed., Tsinghua University Press, Beijing.

Consoli, N. C., Rosa, F. D., and Fonini, A. (2009). "Plate load tests on cemented soil layers overlaying weaker soil." *J. Geotech. Geoenviron. Eng.*, 10.1061/(ASCE)GT.1943-5606.0000158, 1846–1857.

Consoli, N. C., Schnaid, F., and Milititsky, J. (1998). "Interpretation of plate load tests on residual soil site." *J. Geotech. Geoenviron. Eng.*, 10.1061/(ASCE)1090-0241(1998)124:9(857), 857–867.

Costa, Y. D., Cintra, J. C., and Zornberg, J. G. (2003). "Influence of matric suction on the results of plate load tests performed on a lateritic soil deposit." *Geotech. Test. J.*, 26(2), 219–226.

Downloaded from ascelibrary.org by Hohai University Library on 01/17/16. Copyright ASCE. For personal use only; all rights reserved.

Cundall, P. A., and Strack, O. D. L. (1979). "A discrete numerical model for granular assemblies." *Géotechnique*, 29(1), 47–65.
De Beer, E. E. (1965). "Bearing capacity and settlement of shallow foundations on sand." *Proc., Symp. on Bearing Capacity and Settlements of Foundations*, Duke Univ., Durham, NC, 15–33.
Delenne, J.-Y., Youssoufi, M. S. E., Cherblanc, F., and Bénet, J.-C. (2004). "Mechanical behaviour and failure of cohesive granular materials." *Int. J. Numer. Anal. Methods Geomech.*, 28(5), 1577–1594.
Fu, Z. Z., Chen, S. S., and Wang, T. B. (2014). "Discrete element simulation program for earth and rockfill structures (DEAPERS) theory and manual." *Research Rep. Soil 51379130*, Nanjing Hydraulic Research Institute, Nanjing, China.
Fu, Z. Z., and Huo, J. P. (2013). "Utilization of the overburden gravel layer in Tongguankou concrete faced rockfill dam engineering." *Research Rep. Soil 2013040*, Nanjing Hydraulic Research Institute, Nanjing, China.
Fu, Z. Z., Liu, S. H., and Li, Z. (2011). "Discrete element simulations of two wetting effects on granular materials." *Chin. Sci. Bull.*, 56(35), 3803–3811.
Herle, I., and Tejchman, J. (1997). "Effect of grain size and pressure level on bearing capacity of footings on sand." *Proc., Int. Symp. on Deformation and Progressive Failure in Geomechanics*. Elsevier Science Japan, Tokyo, 781–786.
Hermanns, M. (2002). "Parallel programming in Fortran 95 using OpenMP." ⟨http://www.openmp.org/presentations/miguel/F95_OpenMPv1_v2.pdf⟩ (May 30, 2015).
Hettler, A., and Gudehus, G. (1988). "Influence of the foundation width on the bearing capacity factor." *Soils Found.*, 28(4), 81–92.
Hisham, T. E. (2013). "Bearing capacity and settlement of skirted shallow foundations on sand." *Int. J. Geomech.*, 10.1061/(ASCE)GM.1943-5622.0000237, 645–652.
Itasca Consulting Group (1999). *PFC3D particle flow code in three dimensions*, Version 2.00. Minneapolis.
Jiang, X. Q. (2009). "Study on micro-fabric mechanism of soil mailing." Master's thesis, 0630202030, Institute of Hydraulic Structures, Hohai Univ., Nanjing, China.
Kumar, J. (2003). "N_γ for rough strip footing using the method of characteristics." *Can. Geotech. J.*, 40(3), 669–674.
Kumar, J. (2004). "Effect of footing–soil interface friction on bearing capacity factor N_γ." *Géotechnique*, 54(10), 677–680.
Kumar, J. (2009). "The variation of N_γ with footing roughness using the method of characteristics." *Int. J. Numer. Anal. Methods Geomech.*, 33(2), 275–284.
Liu, S. H., and Sun, D. A. (2002). "Simulating the collapse of unsaturated soil by DEM." *Int. J. Numer. Anal. Methods Geomech.*, 26(6), 633–646.
Liu, S. H., Wang, Z. J., Wang, Y. S., Wang, L., and Fu, Z. (2015). "A yield function for granular materials based on microstructures." *Eng. Comp.*, 32(4), 1006–1024.
Liu, S. H., Yao, Y. P., and Sun, Q. C. (2009). "Microscopic study on stress-strain relation of granular materials." *Chin. Sci. Bull.*, 54(23), 4349–4357.
Loukidis, D., and Salgado, R. (2011). "Effect of relative density and stress level on the bearing capacity of footings on sand." *Géotechnique*, 61(2), 107–119.
Matsuoka, H., and Liu, H. (2005). *A new earth reinforcement method using soilbags*. Taylor & Francis, Delft, Netherlands.
Meyerhof, G. G. (1955). "Influence of roughness of base and ground-water conditions on the ultimate bearing capacity of foundations." *Géotechnique*, 5(3), 227–242.
Oh, W. T., and Vanapalli, S. K. (2013). "Scale effect of plate load tests in unsaturated soils." *Int. J. Geomater.*, 4(2), 585–594.
Sanchez, J., Auvinet, G., and Cambou, B. (2015). "Coordination number and geometric anisotropy in binary sphere mixtures." Geomechanics from Micro to Macro, Taylor & Francis, London, 225–230.
Shiraishi, S. (1990). "Variation in bearing capacity factors of dense sand assessed by model loading tests." *Soils Found.*, 30(1), 17–26.
Sloan, S. W. (2013). "Geotechnical stability analysis." *Géotechnique*, 63(7), 531–572.
Smith, G. N., and Smith, I. G. N. (1998). *Elements of soil mechanics*, 7th Ed., Blackwell Science, Oxford, U.K.
Sun, Q. C., and Wang, G. Q. (2009). *Introduction to mechanics of granular materials*, Science Press, Beijing.
Tatsuoka, F., Okahara, M., Tanaka, T, Yang, J.-J., and Liu, F. (1991). "Progressive failure and particle size effect in bearing capacity of a footing on sand." *Geotech. Sepc. Publ.*, 27(2), 788–802.
Terzaghi, K. (1943). *Theoretical soil mechanics*, John Wiley & Sons, New York.
Ueno, K., Miura, K., Kusakabe, O., and Nishimura, M. (2001). "Reappraisal of size effect of bearing capacity from plastic solution." *J. Geotech. Geoenviron. Eng.*, 10.1061/(ASCE)1090-0241(2001)127:3(275), 275–281.
Veiskarami, M., Kumar, J., and Valikhah, F. (2014). "Effect of the flow rule on the bearing capacity of strip foundations on sand by the upper-bound limit analysis and slip lines." *Int. J. Geomech.*, 10.1061/(ASCE)GM.1943-5622.0000324.
Yamaguchi, H., Kimura, T., and Fuji, N. (1976). "On the influence of progressive failure on the bearing capacity of shallow foundations in dense sand." *Soils Found.*, 16(4), 11–22.
Zhang, L., and Thornton, C. (2007). "A numerical examination of the direct shear test." *Géotechnique*, 57(4), 343–354.
Zhu, F., Clark, J. I., and Phillips, R. (2001). "Scale effect of strip and circular footings resting on dense sand." *J. Geotech. Geoenviron. Eng.*, 10.1061/(ASCE)1090-0241(2001)127:7(613), 613–621.

Downloaded from ascelibrary.org by Hohai University Library on 01/17/16. Copyright ASCE. For personal use only; all rights reserved.

AUTHOR QUERY FORM

AQ1: ASCE Open Access: Authors may choose to publish their papers through ASCE Open Access, making the paper freely available to all readers via the ASCE Library website. ASCE Open Access papers will be published under the Creative Commons-Attribution Only (CC-BY) License. The fee for this service is $1750, and must be paid prior to publication. If you indicate Yes, you will receive a follow-up message with payment instructions. If you indicate No, your paper will be published in the typical subscribed-access section of the Journal.

AQ2: Please provide the ASCE Membership Grades for the authors who are members.

AQ3: Note that "plate loading test" was changed to "plate-load test" throughout the article per ASCE style.

AQ4: Please verify the last sentence of the abstract as edited, or edit further if necessary to retain your original meaning.

AQ5: Please add a reference in the list for Cerato et al 2007, or delete the citations from the text (both in this paragraph).

AQ6: This sentence is a bit confusing; please verify that "imitates" is the correct word, or edit as necessary for clarity.

AQ7: Is the change to "credibility" okay/as meant?

AQ8: Please verify changes made to the "In contrast, some..." sentence, or edit further if needed to retain your original meaning.

AQ9: Please edit to clarify what is meant by "simulation of plate-load tests."

AQ10: Please verify edits made to the "Similar to other DEM ..." sentence, or edit further if necessary.

AQ11: Please verify edits made to the "Furthermore, the fact..." sentence, or edit further if necessary.

AQ12: The figures have not been cited sequentially in the text. Please renumber the figures so they are cited in numerical order in the text per journal style.

AQ13: The phrase "which were carried out..." seems out of place here; please edit to clarify what was carried out.

AQ14: Please clarify what "lg" in Eq. (4) represents; if it's a variable, please change to italic type and define it in the following statement, and if it's meant to be "log," please change accordingly.

AQ15: Please verify changes to the "It can be seen..." sentence, or edit further if necessary.

AQ16: Please clarify "both figures" here; do you mean Figs. 4(a and b)?

AQ17: Is the change from "steal" to "steel" okay/as meant? If not, please edit further for clarity.

AQ18: Is the change to a numbered list here (per usual style) okay?

AQ19: Please clarify what "their" references here (or change to "its" if that was meant).

AQ20: Please verify changes to the "Therefore, in laboratory..." sentence, or edit further if necessary.

AQ21: For Bhandar and Han, please provide the name of the publisher and the city of publication.

AQ22: For De Beer, please verify or correct the added location for Duke.

AQ23: For Herle and Tejchman, please provide the publisher's name and location or provide the name of the society that held the symposium.

AQ24: For Hermanns, please provide the last date (month, day, year) on which you accessed the website.

AQ25: For Jiang, please provide a department name, if applicable.

AQ26: For Matsuoka and Liu, please verify or correct the added city of publication.

Downloaded from ascelibrary.org by Hohai University Library on 01/17/16. Copyright ASCE. For personal use only; all rights reserved.